Journal of Marine Science and Technology

Volume 25 | Issue 1 Article 10

# HIGH-FREQUENCY EXCITED NON-PREMIXED JET FLAME IN CROSSFLOW

Richard Kyalo Kimilu
*Department of Mechanical Engineering, National Taiwan University of Science and Technology, Taipei, Taiwan, R.O.C.*

Rong Fung Huang
*Department of Mechanical Engineering, National Taiwan University of Science and Technology, Taipei, Taiwan, R.O.C.*, rfhuang@mail.ntust.edu.tw

Ching Min Hsu
*Department of Mechanical Design Engineering, National Formosa University, Huwei Township, Yunlin County, Taiwan, R.O.C.*



## Recommended Citation

Kimilu, Richard Kyalo; Huang, Rong Fung; and Hsu, Ching Min (2017) "HIGH-FREQUENCY EXCITED NON-PREMIXED JET FLAME IN CROSSFLOW," *Journal of Marine Science and Technology*: Vol. 25: Iss. 1, Article 10.
DOI: 10.6119/JMST-016-0928-1
Available at: https://jmstt.ntou.edu.tw/journal/vol25/iss1/10

Journal of Marine Science and Technology, Vol. 25, No. 1, pp. 96-107 (2017)
DOI: 10.6119/JMST-016-0928-1

# HIGH-FREQUENCY EXCITED NON-PREMIXED JET FLAME IN CROSSFLOW

Richard Kyalo Kimilu[1], Rong Fung Huang[1], and Ching Min Hsu[2]

Key words: excited jet flame, pulsation intensity, wake-stabilized flame, flame control.

## ABSTRACT

A non-premixed jet flame acoustically pulsed at the third resonant frequency of 645 Hz was studied experimentally in a wind tunnel. Flame behavior, characteristics, temperature distributions, and combustion-product distributions were investigated. The flame behavior was characterized by flame visualization. Flame dimensions were obtained from long-exposure flame images. A fine-wire, R-type thermocouple was used to probe temperature distributions while combustion product concentrations were measured using a gas analyzer. Three characteristic flame modes, I, II, and III were identified in the domain of jet pulsation intensity ($I_{pul}$). Mode I flames ($0 \le I_{pul} \le 0.30$) were not affected by pulsation, and remained similar to the non-excited flames. Mode II flames ($0.30 < I_{pul} \le 0.70$) were characterized by a rapidly decreasing flame length, shrinking recirculation flame, and reducing flame luminosity. Mode III flames featured highly unstable, flashing blue flames prior to blow off. Temperature and combustion-product concentrations profiles showed improved mixing as the jet pulsation was increased beyond mode I. Higher temperatures, lower carbon monoxide and slightly reduced nitric oxide concentrations were recorded. Pulsing a jet at a low jet-to-crossflow momentum flux ratio and a jet pulsation intensity above 0.30 resulted in improved combustion.

## I. INTRODUCTION

The jet flame in crossflow is employed in a wide range of applications, such as industrial burners, refinery flaring operations, and gas turbine combustors. In such applications, the flame stability and combustion efficiency are of primary concern because they influence system reliability and effectiveness, and also determine the level of environmental pollution resulting from combustion emissions.

Jets in cross flow are either categorized as *wall-issued* or *stack-issued* depending on whether they are introduced via a wall orifice or a stack protruding into the crossflow, respectively (Gollahalli and Nanjundappa, 1995; Huang and Wang, 1999). The wall-issued jet is mostly influenced by the crossflow and the wall boundary layer, while the stack-issued jet flame is influenced by the crossflow, the tube and jet wakes. Several parameters are used to characterize these flow fields among which are the jet-to-crossflow momentum flux ratio, jet-to-crossflow velocity ratio, jet Reynolds number and the crossflow Reynolds number. The jet-to-crossflow momentum flux ratio $R$ has been found to accurately characterize stack-issued jet flames in crossflow (Kalghatgi, 1981; Huang and Chang, 1994; Gollahalli and Nanjundappa, 1995; Huang and Wang, 1999). At low $R$ below a critical value, the downwash effect of the crossflow in the tube wake as it passes over the burner (stack) tip is appreciable, and the flame is stabilized at the tube wake. Such flames are categorized as burner-attached (or burner-stabilized) jet flames. At large $R$ above a critical value, the flame is detached from the burner and is stabilized at a distance above the horizontal burner plane. Such flames are categorized as liftable flames. The behavior, characteristics, temperature, and chemical structure of stack-issued jet flames have been widely reported over the decades using $R$ as the main scaling parameter (Kuppu Rao and Brzustowski, 1982; Askari et al., 1990; Ellzey et al., 1990; Huang and Sheen, 1996; Huang and Yang, 1996; Savas et al., 1997; Bandaru and Turns, 2000; Birch et al., 2007). Recent works have connected flame stability in crossflow to flame strain rate and differential diffusion of hydrogen gas at the flame base (Kolla et al., 2012; Steinberg et al., 2013; Katta et al., 2015; Wagner et al., 2015). The diffusion flames in crossflow have different mixing and reactive characteristics when compared to diffusion jet flames in quiescent air, and it would be expected their combustion emissions to be different. Whereas shorter flames have been observed for the case of the jet flames in crossflow indicative of enhanced entrainment and mixing, comparative high levels of unburned hydrocarbons and CO emissions have been observed, and similar trends for $NO_X$ when compared to flame in quiescent air (Broadwell and Breidenthal, 1984; Karagozian, 1986; Karagozian and Nguyen, 1988; Bandaru and Turns, 2000). These earlier works conjectured this as a consequence of fuel being swept from the nearfield and local flame

*Paper submitted 05/10/15; revised 08/16/16; accepted 09/28/16. Author for correspondence: Rong Fung Huang (e-mail: rfhuang@mail.ntust.edu.tw).*
*[1] Department of Mechanical Engineering, National Taiwan University of Science and Technology, Taipei, Taiwan, R.O.C.*
*[2] Department of Mechanical Design Engineering, National Formosa University, Huwei Township, Yunlin County, Taiwan, R.O.C.*

quenching resulting from rapid mixing with the crossflow. However, Johnson and Kostiuk (2000) and Johnson et al. (2001) showed that there indeed existed fuel leakage especially at the underside of the flame, which they attributed to the mean flow induced by the standing vortex on the leeside of the stack, and changes in the mean and instantaneous flame structure.

In order to reduce these pollutant emissions and soot from hydrocarbon fuel systems, the fuel can be fully or partially premixed with oxidant and combusted at lean conditions. However, use of premixed fuel mixtures raises safety concerns related to blowout and flashback. These concerns have motivated the exploration of safer alternatives for achieving low emissions and improved combustion efficiency. Jet or flame pulsing has been shown to lower combustion emissions and flame instability. For instance, acoustic pulsing of a combustor at a high-amplitude, low-to-moderate frequency has been shown to lower NO, CO, and soot emissions (Zinn, 1992; Keller et al., 1994; Tang et al., 1995) and high-frequency, low-amplitude acoustic excitation has been used as an active flame instability control mechanism in premixed combustion chambers (Gutmark et al., 1989; Gutmark et al., 1993). Most of these studies employed premixed mixtures. Recent studies on non-premixed straight jet and swirl flow burners have shown that acoustic pulsing can improve flame stability and mixing (and hence combustion efficiency) if appropriate pulsing frequencies and amplitudes are used (Ramamurthi and Patnaik, 2004; Ezekoye et al., 2005; Farhat et al., 2005a; Farhat et al., 2005b; Linck and Gupta, 2007; Chen et al., 2012; Chen et al., 2013).

Few researchers, however, have reported on pulsed jet flames in crossflow. El Behery et al. (2005) reported a reduction in unburned hydrocarbons (UHC), carbon monoxide (CO), and nitric oxide (NO) when applying acoustic pulsing to a stack-issued jet flame in crossflow, while Marr et al. (2012) reported that pulsing of a non-premixed wall-issued jet in cross flow resulted in flames similar to those of fully or partially premixed jets. Whereas Marr et al. (2012) utilized the resonance frequency associated with the burner, El Behery et al. (2005) used a low excitation frequency of 110 Hz. These frequency choices were within the frequency ranges of most straight-jet burner studies. However, little attention has been paid to excitations beyond resonance conditions. Lakshminarasimhan et al. (2006) reported the flame characteristics of straight-jet flames pulsed at the 2nd resonant frequency of 580 Hz. The authors observed that vortices did not emerge from the tube, but were rather drawn back into the fuel tube before they could fully form. They reported that more fine-scale turbulence mixing was associated with the 2nd resonant case than at resonant pulsing.

In the present study, a jet flame in crossflow was pulsed at the tube burner's 3rd resonant frequency (645 Hz). The resulting flame behavior, characteristics, temperature profiles, and combustion products concentration profiles are presented and discussed below. A jet with a low $R$ of 0.192 was pulsed with an amplified acoustic square wave. Jet velocity response to acoustic pulsation at no crossflow at the burner exit plane was characterized using a single-component hot-wire probe. Long-exposure flame images and flame evolution videos were used to delineate flame behavior and characteristics. Flame temperature and combustion product concentrations were probed using a fine-wire thermocouple and a continuous flow multi-gas analyzer.

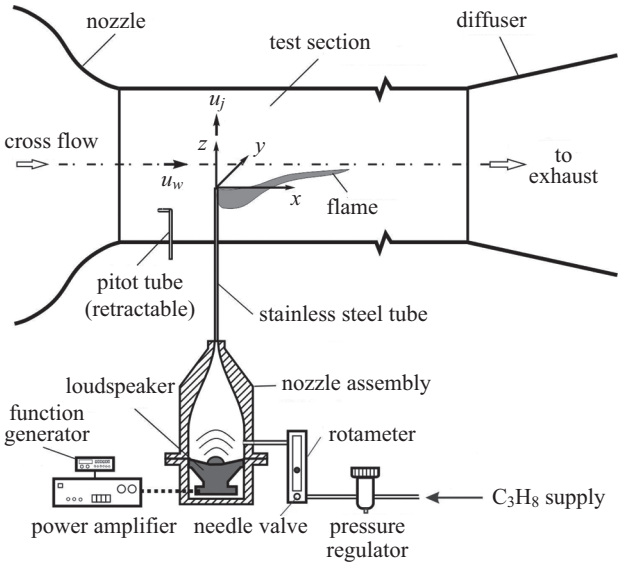


**Fig. 1. Experimental setup.**

## II. EXPERIMENTAL METHODS

### 1. Apparatus

Fig. 1 is a schematic representation of the experimental set up. Experiments were conducted in the test section of an open-loop suction-type wind tunnel. The test section had a square cross-section of 50 × 50 cm and a length of 110 cm. Its walls were made of transparent, heat-resistant glass panels, while the base and roof were made of polished aluminum alloy plates. A variable speed fan located downstream of the test section drew air into the test section and exhausted it to the atmosphere via a square duct. A retractable pitot tube associated with a high-precision electronic pressure transducer was used to measure and monitor the crossflow. A constant crossflow with a Reynolds number ($Re_w$) of 1373 was maintained. The air was conditioned prior to entering the test section by passing it through a honeycomb, wire meshes, and then a convergent nozzle. Low turbulence intensity of less than 0.3% was measured in the test section under the experimental conditions. A computer-controlled three-dimensional traversing mechanism with a step accuracy of 10 μm was mounted on top of the wind tunnel to ensure accurate positioning of probes.

A stainless steel tube with an internal diameter ($d$) of 5 mm, an external diameter ($D$) of 6.4 mm, and a length ($L$) of 545 mm, was used as the burner. It protruded perpendicularly into the test section simulating a stack height ($h$) of 185 mm. The lower end of the burner tube was adapted to a nozzle assembly. The nozzle was 300 mm high, had an inner wall surface contoured to a fifth-order profile, and a contraction ratio of 900. A

loudspeaker used for the jet excitation was fitted at a plenum, downstream of the nozzle-a configuration referred to as "downstream longitudinal irradiation" by Ginevsky et al. (2004). An amplified 50% duty cycle square wave was used to drive the loudspeaker. A Cartesian coordinate system ($x$, $y$, $z$) centered at the tube exit plane was used to describe positions, as shown in Fig. 1.

A commercial grade propane gas (95% $C_3H_8$, 3.5% $C_2H_6$, and 1.5% $C_4H_{10}$) was used as fuel. The gas was stored and passed from a high pressure reservoir past a pressure regulator, a needle valve, and a calibrated rotameter using flexible high-pressure tubing, and fed into the nozzle assembly. A constant jet flow was maintained throughout the experiments corresponding to a jet Reynolds number ($Re_j$) of 1500. The resultant jet-to-crossflow momentum flux ratio $R$ was 0.192.

### 2. Jet Pulsation Velocity Measurements

The response of jet velocity to acoustic excitation was measured at the burner exit under zero crossflow conditions. A one-component hot-wire probe (TSI Inc., Model 1210-T.1.5) was used, and was positioned at ($x/d$, $y/d$, $z/d$) = (0, 0, 0.3). The original tungsten wire was replaced with a platinum wire of 1.5 mm in length and 5 μm in diameter. The replacement was done because the platinum wire had a temperature coefficient of electric resistance more suitable to match the requirement of our Wheatstone bridge of the electronic processor, and also because the platinum wire did not oxidize as fast as the tungsten wire. The dynamic response corresponding to the electronic square wave was adjusted to 20 kHz. Hot-wire output signals were analogue filtered using a low-pass filter having a cut-off frequency of 6 kHz, and fed into a high-speed PC-based data acquisition system for analysis. The sampling and elapse time for data acquisition were set at 10,000 samples/s and 3 s, respectively. The logged data was processed to obtain velocity root-mean-square $u_{j0}'$ values and the power spectral density functions $\Phi$ of the pulsed jet velocity. Jet pulsation intensity ($I_{pul}$) was defined as the ratio of the root-mean-square velocity to the average jet velocity $u_j$.

### 3. Flame Visualization

Long exposure (2 s) flame images were acquired using a Nikon Inc. Model D3200 digital camera. The camera had a 23.2 × 23.2 mm color CMOS sensor, and a maximum resolution of 6016 × 4000 pixels. The photographs were taken at a medium resolution of 4512 × 3000 pixels. Flame behavior was visually inspected with the aid of high speed flame evolution videos. The videos were captured using a high-speed camera (Photron Inc. Model SA3, Type 120K-C2 LCA). The camera had a color CMOS sensor with a maximum resolution of 1024 × 1024 pixels. Videos were recorded at 6000 fps at 512 × 512 pixels and a shutter speed of 0.16 ms. Flame length $l$ and recirculation flame width $w$ were determined by measuring magnified long-exposure flame images. Over 20 frames were measured and averaged. Convergence to within 99% of the average values was obtained within 10-15 images for all experimental conditions.

### 4. Temperature Measurement

The temperature measurements were carried out using a home-made L-shaped R-type (Pt-Pt/13% Rh) thermocouple probe. The probe had a wire diameter of 125 μm and a junction diameter of 175 μm. The wires were fitted in a 1.3 mm diameter ceramic stem, which was securely housed in a stainless tube. The measuring bead protruded 15 mm away from the tip of the ceramic stem. Temperature data was logged using a commercial MX 100 data acquisition unit and processed using standard MX 100 software. The sample rate and record length were 2 Hz and 60 s, respectively.

### 5. Combustion Product Measurements

A multi-gas analyzer (NOVA Inc., Model 7466K) was used to measure the combustion product concentrations of UHC, CO, and NO. The UHC and CO were detected by a single non-dispersive infrared (NDIR) sensor with no moving parts, while NO was detected by a long-life electrochemical sensor. The gas detection ranges for the analyzer were 0-20,000 ppm for UHC, 0-10% for CO, and 0-5000 ppm for NO. Detection resolutions were 1 ppm for UHC and NO, and 0.01% for CO. The probe consisted of an L-shaped stainless steel tube with an inner diameter of 1.8 mm and an outer diameter of 3.2 mm. A suction pump sucked the hot gases past a cooler, a filter, and a dehumidifier into the gas analyzer. Sampled gases were released into the atmosphere via an exhaust tube. An average suction rate of 850 $cm^3$/min was established to minimize suction influence on flame and data authenticity. Probing time was set to 4 minutes for stabilized data recording.

## III. RESULTS AND DISCUSSION

### 1. Jet Velocity Pulsations

Fig. 2 shows the time series of the jet response at the jet exit plane and respective power spectral density functions $\Phi$. At no excitation (not shown), the time series featured a uniform jet velocity at 1.46 m/s while the power spectrum had no predominant peak, or a sloping sub-inertial range. This indicates that the jet did not sync with any preferred natural frequency mode. When the jet was excited at a low pulsation intensity of $I_{pul}$ = 0.11 (Fig. 2(a)), the jet manifested a low amplitude sinusoidal waveform with a period of 1.55 ms, which corresponds to the period of the exciting acoustic square wave signal. The corresponding power spectrum featured a predominant peak at 645 Hz, the frequency of the exciting signal. In this case, then, the jet pulsation frequency synchronized with the exciting frequency. Comparing the velocity signal with the amplifier signal revealed that the jet signal lagged behind by 73% of the wave period. As the pulsation intensity is increased, the jet retained the sinusoidal waveform and period and the amplitude increased, as shown in Figs. 2(b)-(d). At the higher pulsation intensities, the jet phase lag remains constant at 70%. The power density spectral diagrams consistently exhibit a predominant peak at 645 Hz (Figs. 2 (f)-(h)), indicating that the signal cou pling is not

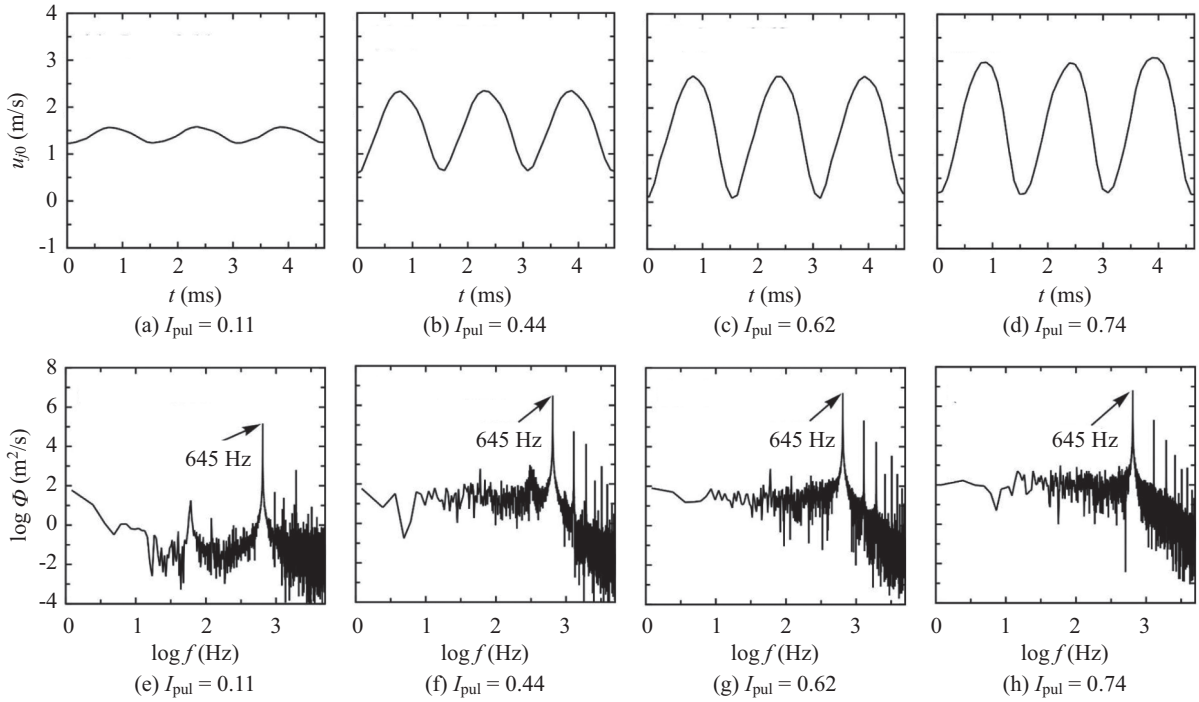


**Fig. 2. Jet velocity response at jet exit plane at zero crossflow. Upper column: time series; Lower column: power spectral density distributions. $f_{exc}$ = 645 Hz, $Re_j$ = 1500.**

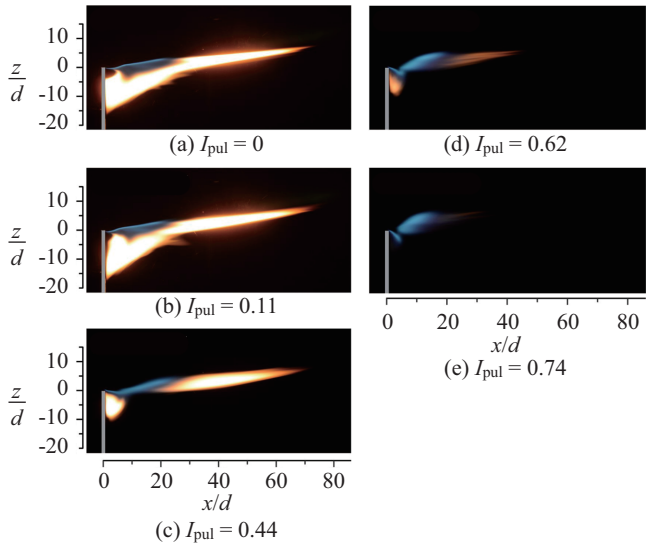


**Fig. 3. Long exposure (2 s) side view flame appearances. (a) non-excited, (b) mode I, (c, d) mode II, (e) mode III flames. $f_{exc}$ = 645 Hz, $Re_j$ = 1500, $Re_w$ = 1373, $R$ = 0.192.**

affected by changes in the jet pulsation intensity. The spectral density distributions feature the canonical sloping inertial range, with no peaks for lower frequencies, indicating that much of the spectral energy is possessed by higher frequency harmonics as opposed to low frequency sub-harmonics of the exciting frequency, and that the jet turns turbulent at even low jet pulsation intensities.

## 2. Flame Characteristic Modes

Fig. 3 shows the side views of long-exposure flame appearances at various jet pulsation intensities. The non-excited jet flame, which corresponds to the category of developing flame (Huang and Chang, 1994), is shown in Fig. 3(a). This flame is characterized by a large, highly luminous recirculating flame in the near tube-wake region, a blue reacting zone flame above the recirculating flame, and a similarly luminous tail flame extending downstream to about $x/d \approx 70$. No clear boundary separating the recirculating flame from the tail flame exists. A thin, bright, blue layer on the top of the blue reacting zone of the flame indicates that it is a diffusion flame. Exciting the flame at pulsation intensities in the range $0 < I_{pul} < 0.30$ did not result in significant flame changes. The flames remained similar to those of the non-excited case, except for a slight lifting of the upper region of the recirculating flame from the tube wall as shown in Fig. 3(b) for a flame at $I_{pul} \approx 0.11$. Flames in this range are designated as *mode I* flames. Fig. 4 shows the variation of the flame length $l$ and recirculation flame width $w$ with jet pulsation intensity $I_{pul}$. The short, back-slashed lines demarcate the boundaries of the characteristic flame mode regions. The flame length in mode I flames increased slightly with increasing pulsation intensity, achieving about a 5.4% flame length increase at $I_{pul} \approx 0.30$. The recirculation flame width remained fairly constant for $I_{pul} < 0.20$, then started to shrink as jet pulsation intensity was increased.

Upon increasing the jet pulsation intensity beyond $I_{pul} \approx 0.30$, the recirculation flame and the tail flame separated, forming a

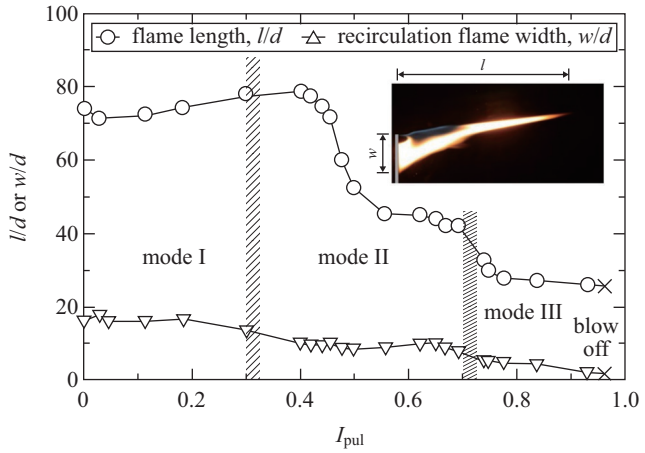


**Fig. 4. Variation of non-dimensional flame length and recirculation flame width with ulsation intensity. $f_{exc}$ = 645 Hz, $Re_j$ = 1500, $Re_w$ = 1373, $R$ = 0.192.**

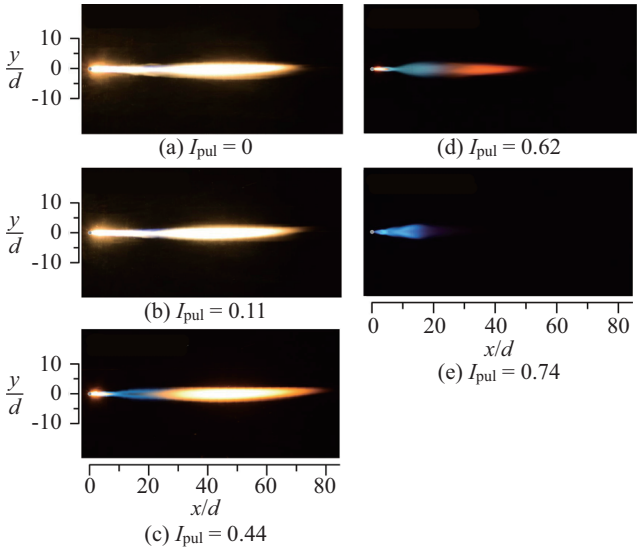


**Fig. 5. Long exposure (2 s) top view flame appearances. (a) non-excited, (b) mode I, (c, d) mode II, (e) mode III flames. $f_{exc}$ = 645 Hz, $Re_j$ = 1500, $Re_w$ = 1373, $R$ = 0.192.**

blue flame neck at about $x/d \approx 18$. The recirculation flame shrank, while the flame length shortened with increasing pulsation intensity. The flame became less luminous and turned fully blue at about $I_{pul} \approx 0.70$. Flames occurring within this jet pulsation intensity range (i.e., $0.30 < I_{pul} < 0.70$) are designated as mode II flames. Fig. 3(b) shows an early stage mode II flame with a blue flame neck and a reduced down-washed recirculation flame at $I_{pul} \approx 0.44$, whereas Fig. 3(c) shows a shortened, almost blue mode II flame at $I_{pul} \approx 0.62$. It is noteworthy that at this later stage of the mode II flames, the near-tube blue flame above the down-washed recirculation flame bent downwards towards the tube wake, while the tail flame formed a conical base aligned with the burner tube top, and extended well above the burner top plane at $x/d > 5$. The tail flame featured a bright blue flame characteristic of a premixed flame. These characteristics tend to suggest that as jet pulsation intensity is increased, combustible mixtures are formed at the upper tube wake (responsible for the base flame), while the gases carried downstream achieve highly mixed combustible ratios further downstream, as indicated by the highly luminous blue flames. Fig. 4 shows that the flame shortens rapidly, especially between $I_{pul} \approx 0.40$ and $I_{pul} \approx 0.55$, beyond which shortening eases as the flame becomes increasingly non-luminous. It is thus inferred that there exists a pulsation intensity below which exciting the jet has insignificant effects on the jet mixing and hence the mode I flames; and above which rigorous mixing occurs, significantly improving the combustion efficiency as indicated by the shortened and blue flames.

At $I_{pul} > 0.70$, fully blue flames occurred. The flames consisted of two parts: a downward-bent base flamelet anchored on the tube tip, and a tail flame which was connected to the base flame by a highly unstable thin flame. The tail flame occasionally detached from the base flame and was swept downstream, exhibiting a 'flashing flame' phenomenon. As the pulsation intensity increased, the flashing became more pronounced and extended farther downstream. Prior to blow off, the flashing ceased, leaving only the base flame, which eventually blew off at about $I_{pul} \approx 0.96$. Flames established at $I_{pul} > 0.70$ are designated as mode III flames. The flashing exhibited at mode III flames may be attributed to jet suction-back at very high jet pulsation intensities above $I_{pul} \approx 0.80$. As the jet is drawn back into the tube and injected out, a leaner premixed mixture results, which was occasionally ignited by the base flame. As premixing increases, close to flame blow-off, the mixture is diluted below the lower lean flammability limit, and the flashing tail flame vanishes. Eventually, the recirculating gases supporting the base flame are also diluted and quenched by the highly premixed gases, and the flame blows off. Lakshminarasimhan et al. (2006) observed that, for a straight jet excited at high frequency (in their case the 2nd resonant frequency of 580 Hz), vortices were not emitted from the tube because they were drawn back into the tube before fully forming; and this was associated with increased fine-scale turbulence. In the present work jet suction-back was observed at $I_{pul} > 0.80$, and hence it could not be responsible for the improved combustion (as a result of in-tube premixing) at lower $I_{pul}$ mode II and III flames. Thus, the high jet velocity fluctuations in mode II and III flames (see Figs. 2(b)-(d)) coupled with the high excitation frequency may have resulted in high fine-scale turbulence mixing, which in turn resulted in improved combustion. The inertial subrange exhibited fully turbulent flow at these pulsation intensities, as shown in Figs. 2(f)-(h).

Fig. 5 shows the top view of flame appearances corresponding to Fig. 3. For non-excited and mode I flames (Figs. 5(a) and (b)), no blue flames are visible on account of the wider, highly luminous recirculating flames under the blue flame reacting zone. At mode II (Fig. 5(c)), the blue flame neck is evident, and the flame width is narrower in the near tube region than in Figs. 5(a) and (b). At $I_{pul} \approx 0.62$ (Fig. 5(d)), a very narrow

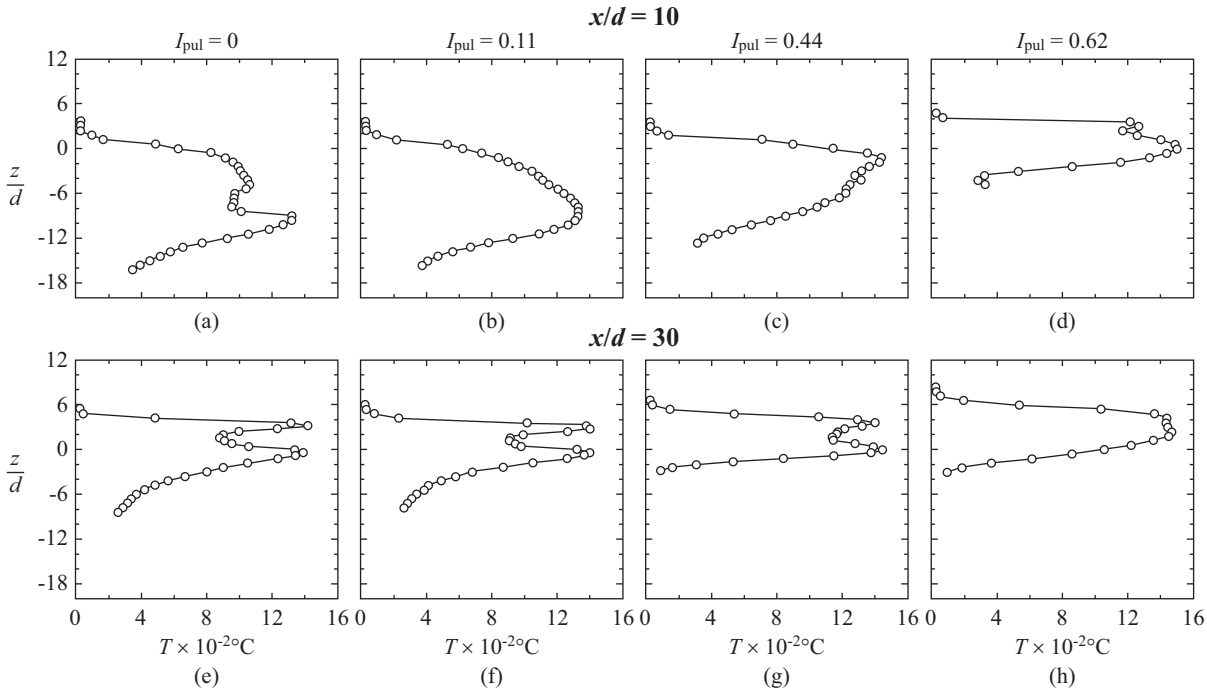


**Fig. 6. Flame temperature distributions at mid-plane ($y/d = 0$). Upper column: $x/d = 10$; Lower column: $x/d = 30$. (a, e) non-excited, (b, f) mode I, (c-h) mode II flames. $f_{exc} = 645$ Hz, $Re_j = 1500$, $Re_w = 1373$, $R = 0.192$.**

flame appears at $x/d < 10$, then the flame fans out at the blue flame region, consistent with the conical shape seen in Figs. 3(d) and 5(d). Fig. 5(e) exhibits a fully fanned flame from the flame base. From these results it can be concluded that pulsating the jet at $I_{pul} > 0.30$ results in gradual flame width narrowing in the near tube region, while the tail flame spreading point moves towards the tube plane.

## 3. Temperature Distributions

Fig. 6 shows the mid-plane flame temperature distribution profiles probed at near- and far-tube flame regions at $x/d = 10$ and 30, respectively. In the non-excited case, the flame features a dual-hump temperature profile at the near-tube flame region, as shown in Fig. 6(a). This profile has been observed by earlier researchers (Gollahalli and Nanjundappa, 1995; Savas et al., 1997) and is associated with the recirculating diffusion flame in the tube-wake vortex formed as a result of the downwashing effect of the crossflow passing over the tube top. The humps demarcate the upper and lower vortex boundaries in the $x$-$z$ plane. At an increased jet pulsation intensity of $I_{pul} \approx 0.11$ corresponding to a mode I flame, the dual-hump featured in the non-excited case is absent, with a more Gaussian-like profile indicating a more premixed flame as opposed to a diffusion flame as in the non-excited case. Higher temperatures are registered on the lower edge of the flame, indicating that the fuel mixing in the recirculating vortex improves downwards. Pulsating the jet at low pulsation intensities appears to improve the air entrained in the tube-wake area, thus improving the fuel mixture by 0.5% over the non-excited case. At $I_{pul} \approx 0.44$, a narrower Gaussian-like profile is observed, but with the peak temperatures occurring on the upper edge of the flame. As discussed earlier, intense mixing occurs in mode II flames. These mixtures are closer to optimal on the upper flame side, owing to increased turbulence mixing on the upper bent jet shear-layer. A narrower profile is expected as this location lies on the flame neck discussed in Section 2 above. Temperatures are 9% higher in this case, reaching 1436°C. At $I_{pul} \approx 0.62$, maximum temperatures of 1500°C are achieved, an improvement of 14% compared to the non-excited case. The profile is narrow as a result of shrinking recirculating flame in the near tube-wake region. Highly turbulent premixed jet flow results in these high flame temperatures. It can thus be concluded that, at the near tube region, flame temperatures increase with increasing jet pulsation indicating an improved combustion efficiency.

Further downstream at $x/d \approx 30$, the flames manifest symmetric dual peak temperature profiles for all pulsation intensities lower than 0.60 (Figs. 6(e) and (f)). These profiles are characteristic of axisymmetric diffusion flames (Gollahalli and Nanjundappa, 1995; Savas et al., 1997). Above this threshold, more Gaussian-like profiles are manifested as observed, for example, at $I_{pul} \approx 0.62$ (Fig. 6(h)). Maximum temperatures improve by a small margin, reaching 1470°C at $I_{pul} \approx 0.62$, which represents a 3.5% increase. It is noteworthy that for flames at $I_{pul} < 0.60$, higher flame temperatures are achieved at $x/d = 30$ compared to those at $x/d = 10$ for corresponding jet pulsation intensities. Beyond $I_{pul} \approx 0.60$, maximum temperatures are achieved closer to the tube. At low to medium jet pulsation intensities, the flame is relatively long, with $x/d = 30$ located

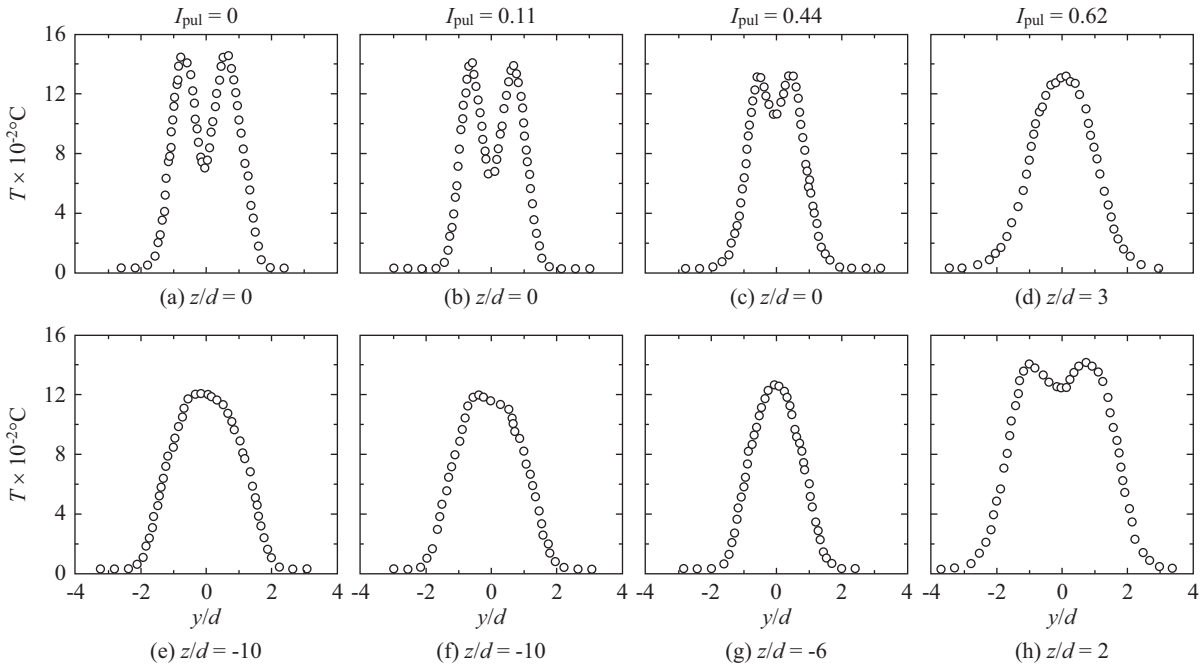


**Fig. 7. Lateral flame temperature distributions at axial distance $x/d$ = 10. (a, e) non-excited, (b, f) mode I, and (c, g, d, h) mode II flames. $f_{exc}$ = 645 Hz, $Re_j$ = 1500, $Re_w$ = 1373, $R$ = 0.192.**

mid-span of the flame, slightly beyond the tip of the blue reacting flame zone. In this region, high-temperature lean mixture combustion occurs at the flame surfaces, resulting in the dual high-temperature peaks observed. Low-temperature combustion product gases from the reaction zone are entrained in the bulk of the flame and are responsible for the dip between the peaks, as will be observed in the next section. At higher jet pulsation intensities, $x/d \approx 30$ is located closer to the flame tip, with more uniform lower temperature combustion gases predominating, thus producing the Gaussian-like profile at $I_{pul} \approx 0.62$. Temperature probing at higher jet pulsation did not yield further temperature increases at both near- and far-tube flame regions.

Fig. 7 shows the lateral temperature profiles at $x/d$ = 10. For flames in the range of $I_{pul} < 0.60$, two types of temperature profiles exist: a dual-peak and Gaussian-like profile on the upper and lower regions of the flames, respectively, as shown in Figs. 7(a)-(f). For the non-excited case, the dual peak extends to about $z/d \approx$ -9.0, below which the Gaussian profile predominates. At $I_{pul} \approx 0.11$, as already observed, there is a slight improvement in combustion, and the dual peak extends to about $z/d \approx$ -8. At $I_{pul}$ = 0.44, the dual-peaks do not persist deep into the flame, as they cease to manifest at $z/d \approx$ -0.5. The dual-peaks observed in this region of the flame are consistent with the two-planar flames observed by Gollahalli and Nanjundappa (1995) for burner-attached flames with recirculating flames in the tube wake. Comparing these results with Figs. 6(a)-(c), it is observed that the dual-peak profiles are conistently exhibited at levels above the maximum temperature level. At $I_{pul}$ = 0.62, three profiles are exhibited; two Gaussian-like profiles on the upper and lower regions of the flame, with dual peaks between them. The dual-peak exists within a short flame width, i.e., $1.5 \leq z/d \leq 2.5$, and seems to match the small temperature dip observed in Fig. 6(d).

Typical lateral temperature profiles at $x/d$ = 30 are shown in Fig. 8. For $I_{pul} < 0.60$, the flames manifest three temperature profiles that are consistent with the axisymmetric flames in this region, i.e., Gaussian-like profiles at upper and lower flame regions, and a dual-peak profile with a dip corresponding to the cooler flame core at middle region of the flame, as shown in Figs. 8(a)-(i). At $I_{pul} \approx 0.62$, the flame manifests Gaussian-like profiles at all levels, as shown in Figs. 8(j)-(l), which is consistent with Fig. 6(h). By comparing the profiles in Figs. 7 and 8, it can be observed that at $x/d$ = 10, pulsing does not lead to significant flame spread, unlike at $x/d$ = 30 where the flame spreads with increasing jet pulsation intensity.

## 4. Combustion Products Concentration Distributions

The concentrations of UHC, CO and NO were probed along the mid-plane ($y/d$ = 0) of the flame. Fig. 9 shows the UHC concentration profiles at $x/d$ = 10. The maximum concentration occurs at $z/d \approx 1.2$ for $I_{pul}$ = 0 and $I_{pul}$ = 0.11, $z/d \approx 1.5$ at $I_{pul}$ = 0.44, and at $z/d \approx 3.0$ for $I_{pul}$ = 0.62. This shows that the fuel jet flow remains un-affected at low jet pulsation intensities. This seems to be in agreement with the unchanging flame characteristics in mode I and early stages of mode II flames (i.e., flames at $I_{pul} < 0.40$). Within the mode II flames jet pulsation range, the maximum UHC position shifts upwards, signifying that the jet penetrates deeper into the crossflow before it is bent and transported downstream by the crossflow. This obviously leads to increased jet-crossflow mixing, which leads

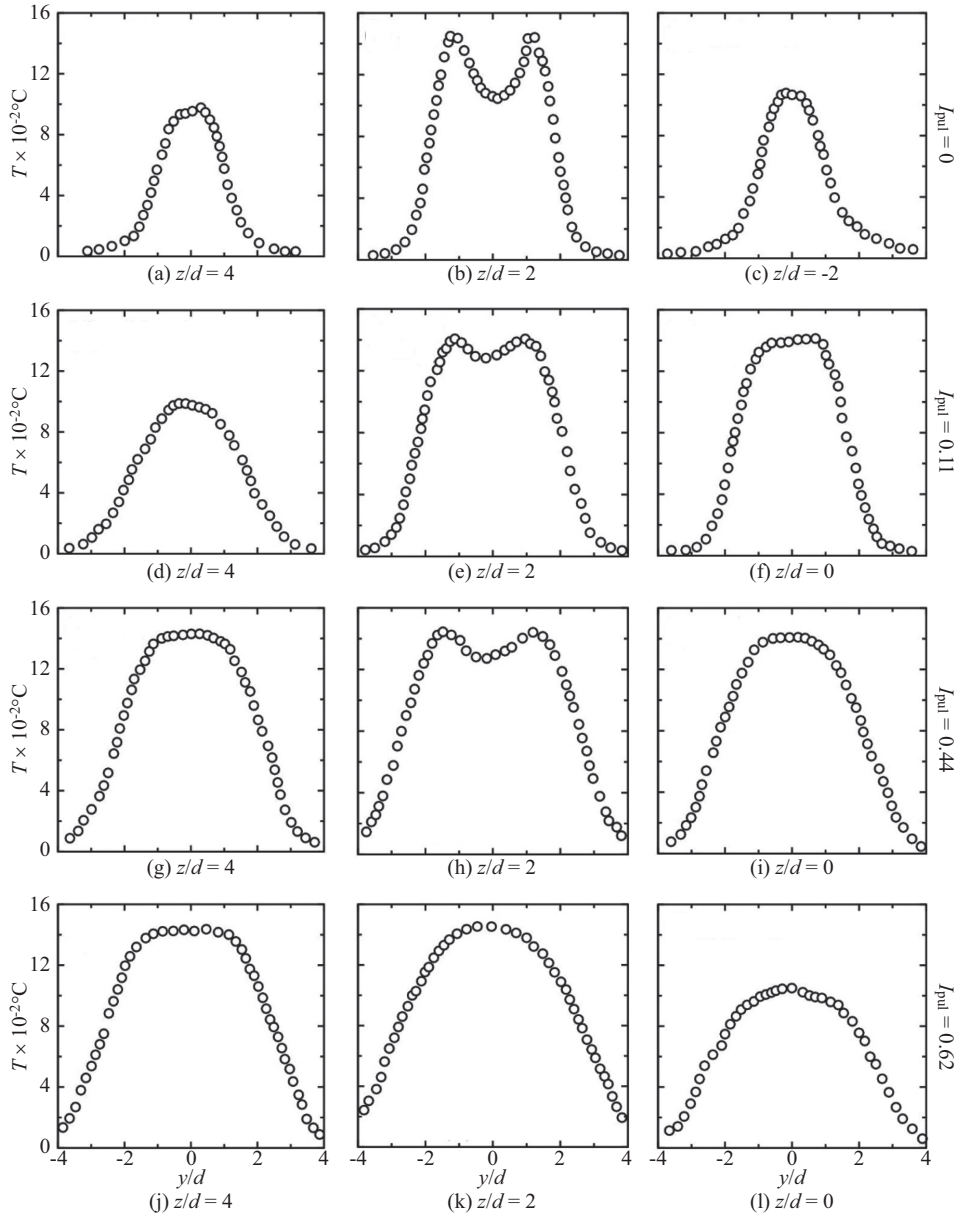


**Fig. 8. Lateral flame temperature distributions at axial distance x/d = 30. (a-c) non-excited, (d-f) mode I, (g-l) mode II flames. $f_{exc}$ = 645 Hz, $Re_j$ = 1500, $Re_w$ = 1373, R = 0.192.**

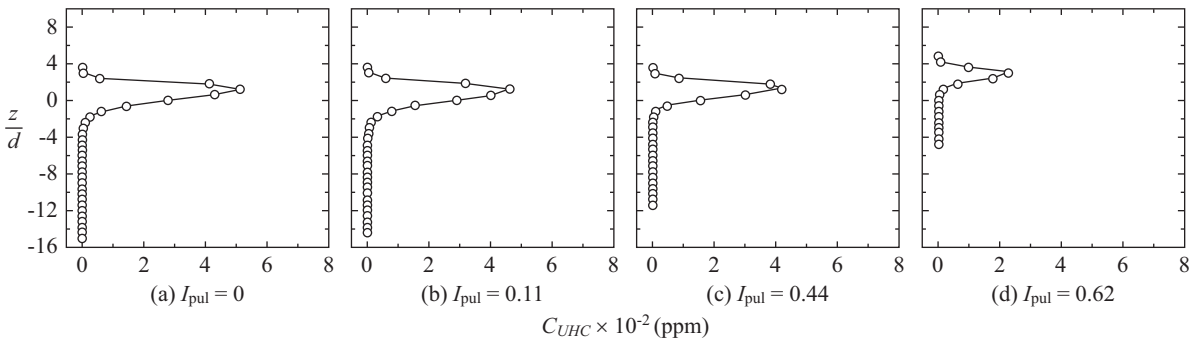


**Fig. 9. Mid-plane ($y/d$ = 0) UHC concentration distributions at axial distance $x/d$ = 10. (a) non-excited, (b) mode I, and (c-d) mode II flames. $f_{exc}$ = 645 Hz, $Re_j$ = 1500, $Re_w$ = 1373, $R$ = 0.192.**

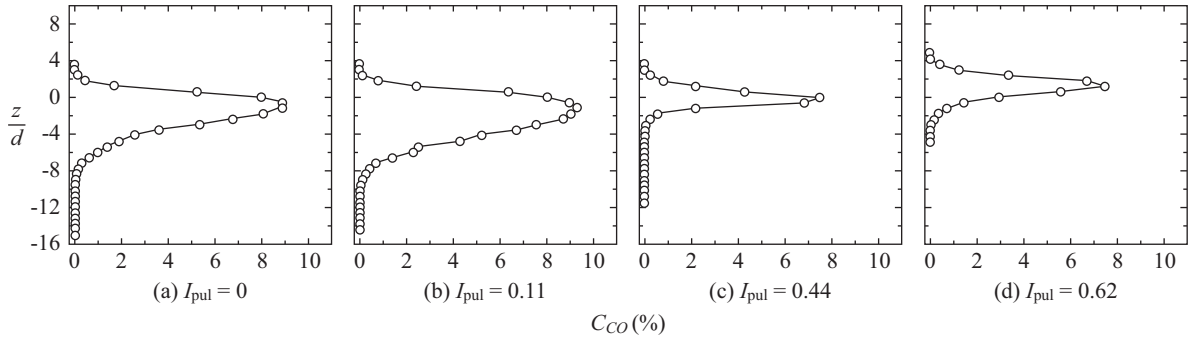


**Fig. 10. Mid-plane ($y/d$ = 0) CO concentration distributions at axial distance $x/d$ = 10. (a) non-excited, (b) mode I, and (c, d) mode II flames. $f_{exc}$ = 645 Hz, $Re_j$ = 1500, $Re_w$ = 1373, $R$ = 0.192.**

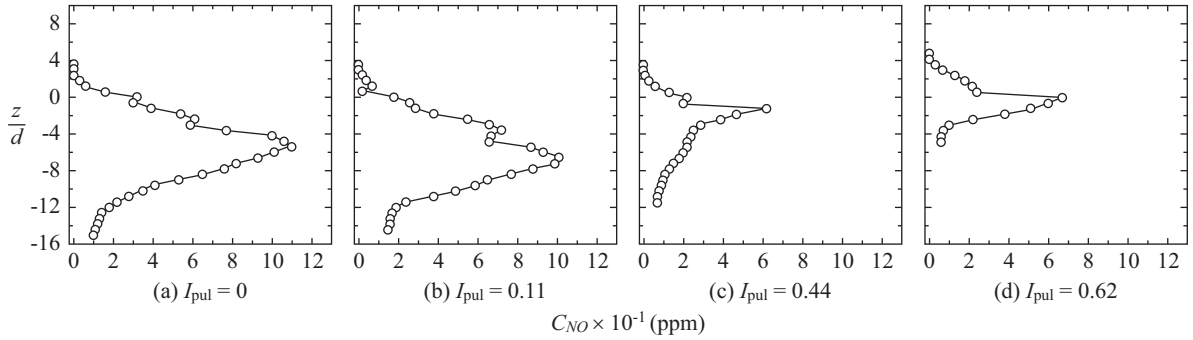


**Fig. 11. Mid-plane ($y/d$ = 0) NO concentration distributions at axial distance $x/d$ = 10. (a) non-excited, (b) mode I, and (c, d) mode II flames. $f_{exc}$ = 645 Hz, $Re_j$ = 1500, $Re_w$ = 1373, $R$ = 0.192.**

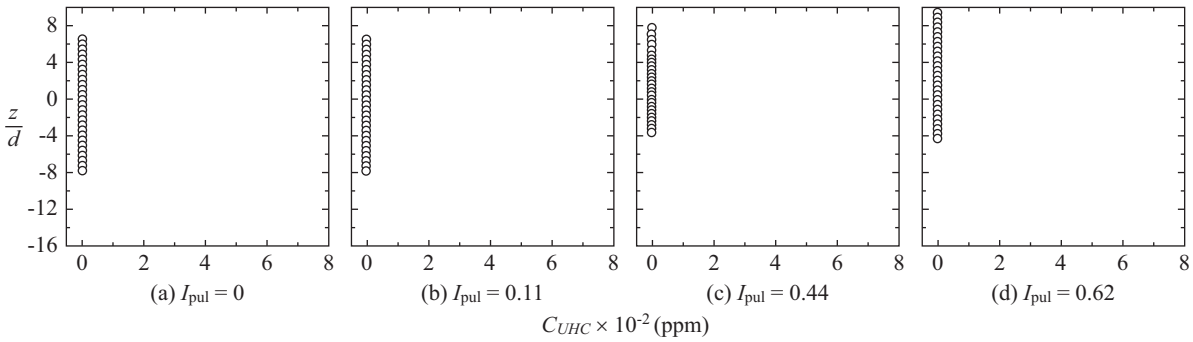


**Fig. 12. Mid-plane ($y/d$ = 0) UHC concentration distribution profiles at axial distance $x/d$ = 30. (a) non-excited, (b) mode I, and (c-d) mode II flames. $f_{exc}$ = 645 Hz, $Re_j$ = 1500, $Re_w$ = 1373, $R$ = 0.192.**

to the improved combustion resulting in the shortened and blue mode II flames (Figs. 3(c) and (d), 4, and 5(c) and (d)). The profiles exhibit a downward trend in the maximum concentration levels. In the non-excited case, the peak value is about 514 ppm, which reduces to about 227 ppm at $I_{pul} \approx 0.62$, signifying a 56% fuel depletion. This indicates that pulsing improves mixing and causes more fuel to combust closer to the burner.

Fig. 10 shows the corresponding CO concentration profiles at $x/d$ = 10. As with UHC, pulsing leads to reduction of CO production, but at a lower improvement of about 19%. Positions of maximum CO are consistently lower than those of UHC for all jet pulsation intensities, indicating that at this axial distance the bulk of the fuel exists above the flame. The NO concentration profiles are as shown in Fig. 11. High NO concentrations were registered in non-excited flames (i.e., about 110 ppm), and diminished with increasing jet pulsation intensity. The minimum NO concentrations of about 62 ppm were recorded at $I_{pul} \approx 0.44$, a 44% reduction. At $I_{pul}$ = 0.62, slightly higher NO concentrations of about 67 ppm were recorded, which is in accordance with expectations for increased flame temperatures.

At $x/d$ = 30, the UHC profiles shown in Fig. 12 depict in-

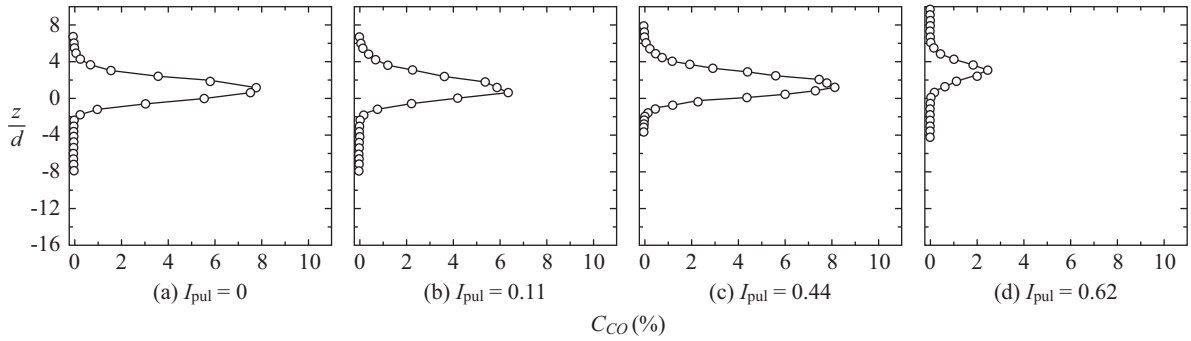


**Fig. 13. Mid-plane ($y/d$ = 0) CO concentration distribution profiles at axial distance $x/d$ = 30. (a) non-excited, (b) mode I, and (c-d) mode II flames. $f_{exc}$ = 645 Hz, $Re_j$ = 1500, $Re_w$ = 1373, $R$ = 0.192.**

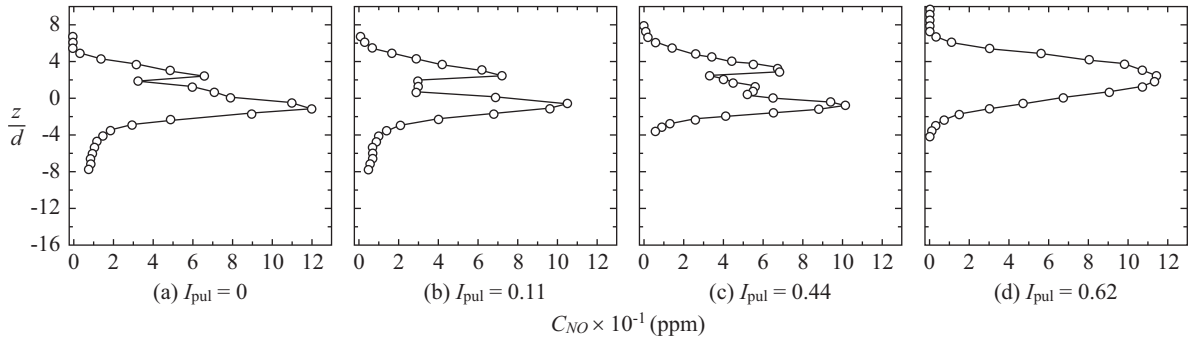


**Fig. 14. Mid-plane ($y/d$ = 0) NO concentration distribution profiles at axial distance $x/d$ = 30. (a) non-excited, (b) mode I, and (c-d) mode II flames. $f_{exc}$ = 645 Hz, $Re_j$ = 1500, $Re_w$ = 1373, $R$ = 0.192.**

significant concentration levels. In the non-excited case, maximum UHC concentrations were about 4 ppm, which is a 99% depletion compared to values at $x/d$ = 10. Jet pulsation reduces levels to about 2 ppm in mode I flames, and negligible trace concentrations (i.e., 0.2 ppm) at mode II flames. The CO concentration profiles are shown in Fig. 13. The profiles feature relatively high concentrations of 8.0, 6.3, and 8.1% at $I_{pul}$ = 0, 0.11 and 0.44, respectively. The peak concentration locations remotely follow the dip observed in the temperature profiles of Figs. 6(e)-(g). At $I_{pul}$ = 0.62, very low CO concentrations of 2.5% are recorded. This represents a 67% reduction compared to the non-excited case. Compared to corresponding CO values at $x/d$ = 10, values at $x/d$ = 30 are generally lower for all pulsation intensities. This is expected as more oxygen is entrained downstream, leading to oxidation of CO to $CO_2$. Fig. 14 shows the NO profiles at $x/d$ = 30. The profiles feature dual peaks akin to those seen in the temperature profiles for $I_{pul}$ = 0, 0.11 and 0.44, and a Gaussian-like profile for $I_{pul}$ = 0.62. Jet pulsation slightly reduces the NO concentrations from 120 ppm for non-excited flames to 101 ppm at $I_{pul} \approx 0.44$ (a 16% reduction), then increases again to about 114 ppm at $I_{pul}$ = 0.62. Downstream, more air is entrained leading to lean mixtures, in which the high nitric oxide emissions are frozen before they can be oxidized, as indicated by the increased NO concentrations. These results indicate that a significant drop in CO emissions is achieved at high jet pulsation intensities, but that NO concentrations remain largely unabated in the downstream region of the flame.

## IV. CONCLUSIONS

Exciting a low $R \approx 0.192$ non-premixed jet flame in crossflow at a high excitation frequency of 645 Hz resulted in significant changes in flame appearance, temperature, and combustion products concentration distributions. The following conclusions were drawn from the experimental results.

(1) Three characteristic flame modes were identified in the domain of jet pulsation intensity. Mode I flames for $I_{pul} < 0.30$, mode II flames for $0.30 < I_{pul} < 0.70$, and mode III flames at $I_{pul} > 0.70$, until flame blow off at about $I_{pul} \approx 0.96$.
(2) Exciting the jet at mode I yielded no significant changes in flame appearances. In mode II, flames were significantly reduced in length and became highly non-luminous, owing to improved mixing and hence improved combustion efficiency. At mode III, the jet acquired high lean mixtures, resulting in highly flashing blue flames prior to blow-off.
(3) Flame temperature distribution profiles showed that jet pulsation led to more premixed flames in the near-tube flame region.
(4) CO emissions were significantly reduced by jet pulsation, unlike NO emissions which remain high, especially in the region far downstream.

(5) Exciting the jet at mode II flames resulted in desirable short, high temperature, and low emission flames that are ideal for combustion applications. Though there is no significant reduction in NO emissions, the levels obtained are lower than for non-excited cases, and hence pose no additional pollution concerns.

## NOMENCLATURE

| | |
|---|---|
| $d$ | inner diameter of tube, 5 mm. |
| $D$ | outer diameter of tube, 6.4 mm. |
| $h$ | burner tube height, 185 mm. |
| $I_{pul}$ | jet pulsation intensity ($= u_{jo}'/u_j$). |
| $L$ | burner tube length, 545 mm. |
| $l$ | ensemble-averaged flame length. |
| $R$ | jet-to-crossflow momentum flux ratio ($= \rho_j u_j^2/\rho_w u_w^2$). |
| $Re_j$ | exit Reynolds number of jet ($= u_j d/v_j$). |
| $Re_w$ | free-stream Reynolds number of crossflow ($= u_w D/v_w$). |
| $t$ | evolving time, s. |
| $T$ | temperature, °C. |
| $u_j$ | average exit velocity of jet based on rotameter calibration. |
| $u_w$ | free-stream velocity of crossflow. |
| $u_{j0}'$ | RMS value of the jet pulsation velocity at exit under zero-crossflow condition. |
| $w$ | ensemble-average recirculation flame width. |
| $x$ | Cartesian coordinate in axial direction. |
| $y$ | Cartesian coordinate in transverse direction. |
| $z$ | Cartesian coordinate in burner tube axis direction. |
| $\rho_j$ | density of jet fluid, 1.812 kg/m$^3$ at 28°C and 1 atm. |
| $\rho_w$ | density of crossflow air, 1.178 kg/m$^3$ at 28°C and 1 atm. |
| $v_j$ | kinematic viscosity of jet fluid, $4.596 \times 10^{-6}$ m$^2$/s at 28°C and 1 atm. |
| $v_w$ | kinematic viscosity of crossflow air, $1.819 \times 10^{-5}$ m$^2$/s at 28°C and 1 atm. |
| $\Phi$ | power spectrum energy density function, m$^2$/s. |

## REFERENCES


Askari, A., S. J. Bullman, M. Fairweather and F. Swaffield (1990). The concentration field of a turbulent jet in a cross-wind. Combustion Science and Technology 73, 463-478.

Bandaru, R. V. and S. R. Turns (2000). Turbulent jet flames in a crossflow-effects of some jet, crossflow, and pilot flame parameters on emmisions. Combustion and Flame 121, 137-151.

Birch, A. D., D. R. Brown, M. Fairweather and G. K. Hargrave (2007). An experimental study of a turbulent natural gas jet in a cross-flow. Combustion Science and Technology 66, 217-232.

Broadwell, J. E. and R. E. Breidenthal (1984). Structure and mixing of a transverse jet in incompressible flow. Journal of Fluid Mechanics 148, 405-412.

Chen, L.-W., Q. Wang and Y. Zhang (2012). Flow characterisation of diffusion flame in a standing wave. Experimental Thermal and Fluid Science 41, 84-93.

Chen, L.-W., Q. Wang and Y. Zhang (2013). Flow characterisation of diffusion flame under non-resonant acoustic excitation. Experimental Thermal and Fluid Science 45, 227-233.

El Behery, R. E., A. A. Mohamad and M. M. Kamal (2005). Combustion enhancement of a gas flare using acoustical excitation. Combustion Science and Technology 177, 1627-1659.

Ellzey, J. L., J. G. Berbe, E. Z. F. Tay and D. E. Foster (1990). Total soot yield from a propane diffusion flame in cross-flow. Combustion Science and Technology 71, 41-52.

Ezekoye, O. A., K. M. Martin and F. Bisetti (2005). Pulsed flow modulation of soot production in a laminar jet-diffusion flame. Proceedings of the Combustion Institute 30, 1485-1492.

Farhat, S., D. Kleiner and Y. Zhang (2005a). Jet diffusion flame characteristics in a loudspeaker-induced standing wave. Combustion and Flame 142, 317-323.

Farhat, S. A., W. B. Ng and Y. Zhang (2005b). Chemiluminescent emission measurement of a diffusion flame jet in a loudspeaker induced standing wave. Fuel 84, 1760-1767.

Ginevsky, A. S., Y. V. Vlasov and R. K. Karavosov (2004). Acoustic control of turbulent jets, Springer-Verlag, Berlin Heidelberg.

Gollahalli, S. R. and B. Nanjundappa (1995). Burner wake stabilized gas jet flames in cross-flow. Combustion Science and Technology 109, 327-346.

Gutmark, E., T. P. Parr, D. M. Hanson-Parr and K. C. Schadow (1989). On the role of large and small-scale structures in combustion control. Combustion Science and Technology 66, 107-126.

Gutmark, E., T. P. Parr, D. M. Hanson-Parr and K. C. Schadow (1993). Structure of a controlled ducted flame. Combustion Science and Technology 87, 217-239.

Huang, R. F. and J. M. Chang (1994). The stability and visualized flame and flow structures of a combusting jet in crossflow. Combustion and Flame 98, 267-278.

Huang, R. F. and H.-J. Sheen (1996). The flow and thermal structure of a turbulent combusting jet in crossflow. Journal of Energy Chinese Society of Mechanical Engineers 17, 343-351.

Huang, R. F. and S. M. Wang (1999). Characteristic flow modes of a wake-stabilized jet flames in a transverse air stream. Combustion and Flame 117, 59-77.

Huang, R. F. and M. J. Yang (1996). Thermal and concentration fields of burner-attached jet flames in crossflow. Combustion and Flame 105, 211-224.

Johnson, M. R. and L. W. Kostiuk (2000). Efficiencies of low-momentum jet diffusion flames in crosswinds. Combustion and Flame 123, 189-200.

Johnson, M. R., D. J. Wilson and L. W. Kostiuk (2001). A fuel stripping mechanism for wake-stabilized jet diffusion flames in crossflow. Combustion Science and Technology 169, 155-174.

Kalghatgi, G. T. (1981). Blow-out stability of gaseous jet diffusion flames part II: effect of cross wind. Combustion Science and Technology 26, 241-244.

Karagozian, A. R. (1986). The flame structure and vorticity generated by a chemically reactingtransverse jet. AIAA Journal 24, 1502-1507.

Karagozian, A. R. and T. T. Nguyen (1988). Effects of heat release and flame distortion in the transverse fuel jet. Symposium (International) on Combustion 21, 1271-1279.

Katta, V. R., D. L. Blunck, N. Jiang, A. Lynch, J. R. Gord and S. Roy (2015). On flames established with air jet in cross flow of fuel-rich combustion products. Fuel 150, 360-369.

Keller, J. O., T. T. Bramlette, P. K. Barr and J. R. Alvarez (1994). $NO_x$ and CO emissions from pulse combustor operating in lean premixed mode. Combustion and Flame 99, 460-466.

Kolla, H., R. W. Grout, A. Gruber and J. H. Chen (2012). Mechanisms of flame stabilization and blowout in a reacting turbulent hydrogen jet in cross-flow. Combustion and Flame 159, 2755-2766.

Kuppu Rao, V. and T. A. Brzustowski (1982). Tracer studies of jets and diffusion flames in Cross-Flow. Combustion Science and Technology 27, 229-239.

Lakshminarasimhan, K., N. T. Clemens and O. A. Ezekoye (2006). Characteristics of strongly-forced turbulent jets and non-premixed jet flames. Experiments in Fluids 41, 523-542.

Linck, M. and A. K. Gupta (2007). Passive control of forced combustion instability in a swirl-stabilized spray combustor. Journal of Propulsion and Power 23, 1113-1122.

Marr, K. C., N. T. Clemens and O. A. Ezekoye (2012). Mixing characteristics and emissions of strongly-forced non-premixed and partially-premixed jet flames in crossflow. Combustion and Flame 159, 707-721.

Ramamurthi, K. and R. E. Patnaik (2004). Noise reduction in non-premixed lifted jet flames. Flow, Turbulence and Combustion 72, 49-67.

Savas, O., R. F. Huang and S. R. Gollahalli (1997). Structure of the flow field of a non-premixed gas jet flame in crossflow. Journal of Energy Resources

Technology 119, 137-144.

Steinberg, A. M., R. Sadanandan, C. Dem, P. Kutne and W. Meier (2013). Structure and stabilization of hydrogen jet flames in cross-flows. Proceedings of the Combustion Institute 34, 1499-1507.

Tang, Y. M., G. Waldherr, J. I. Jagoda and B. T. Zinn (1995). Heat release timing in a nonpremixed helmholtz pulse combustor. Combustion and Flame, 100, 251-261.

Wagner, J. A., S. W. Grib, M. W. Renfro and B. M. Cetegen (2015). Flowfield measurements and flame stabilization of a premixed reacting jet in vitiated crossflow. Combustion and Flame 162, 3711-3727.

Zinn, B. T. (1992). Pulse combustion: recent applications and research issues. Proceedings of the Combustion Institute 24, 1297-1305.